Backscattering measurements from double-scale randomly rough surfaces

Víctor Ruiz-Cortés[1,*] and Christopher Dainty[2]

[1]*Depto. de Óptica, División de Física Aplicada, Centro de Investigación Científica y de Educación Superior de Ensenada (CICESE), Carr. Ensenada-Tijuana No. 3918, Zona Playitas, 22860 Ensenada, B.C., Mexico*
[2]*Applied Optics Group, National University of Ireland, Galway, University Rd., Galway, Ireland*
**Corresponding author: vruizc@cicese.mx*

Received March 12, 2012; revised April 4, 2012; accepted April 4, 2012;
posted April 5, 2012 (Doc. ID 164524); published June 1, 2012

We present experimental measurements of light backscattered from double-scale randomly rough surfaces (ocean-like surfaces) with different statistical parameters illuminated at small and large angles of incidence. The surfaces are composed of a small-scale roughness superimposed on a slowly (large-scale) varying surface. The large-scale surfaces are diamond-machined periodic surfaces made on aluminum substrates and have either a sinusoidal or a Stokes wave profile. The small-scale roughness is added with lithographic techniques, and the surfaces are then gold coated. For a linearly polarized incident beam, it is found that the backscattered light is strongly depolarized mainly at small angles of incidence and strong shadowing effects are present for large angles of incidence ($\theta_{inc} > 60°$).

OCIS codes: 290.0290, 290.5880.

1. INTRODUCTION

The interaction between light and matter has been studied for many years. The reflection and refraction of light from a plane surface of any material are well-known phenomena, and it is possible to obtain information about material properties by analyzing the reflected and refracted light. However, the interaction of light with a rough surface is, in general, not a completely understood problem.

The scattering of waves (e.g., electromagnetic or mechanical) can be utilized in several fields to determine properties of the surface or material of physical bodies. Optical tomography [1], remote sensing [2,3], microscopy [4,5], and surface characterization [6,7] are some of these applications.

The problem of light scattering by rough surfaces has been a subject of continuous interest due to the wide range of applications and important associated phenomena, such as enhanced backscattering [8,9]. Significant advances have been made in the study of light scattered from rough surfaces using different approaches, such as the Kirchhoff boundary conditions [10,11], the small perturbation method [12], and the integral-equation method [13,14].

Special attention has been paid to multiple scattering effects at normal incidence and not very large angles of incidence (up to approx. 50° from the normal) [15–17]. Little work has been done at grazing incidence where the current theories fail (angles of incidence greater than 60°). Numerical simulations in this area involve excessively time-consuming computer programs. Furthermore, available experimental data at such angles of incidence do not include accurate information about the surface structure.

There has been a surging interest in the scattering of waves from multiple scale (composite) surfaces due to its application in remote sensing and radar imaging [18–24]. Radar scattering from the sea surface, particularly at large angles of incidence from the normal, remains a poorly understood phenomenon. One of the main problems is the modeling of the sea surface itself [3]. The most common way to represent the sea surface is to treat it as composed of small capillary waves riding on top of larger gravity waves [22,25–27]. Experimental studies in this area would contribute to a better understanding of scattering by a sea surface and terrain and would help to develop models that could reproduce the features of radar scattering.

Some work has been done in the measurement of the backscattered light from randomly rough surfaces, mainly at small angles of incidence [9,15,17,28]. However, to our knowledge, little work has been reported on backscattering measurements in the full range from normal to grazing incidence. Renau and Collinson [29] and Renau *et al.* [30] measured the optical backscattering from rough surfaces made from different materials (aluminum, magnesium oxide, gold, silver, etc.). They compared the characteristics of the angular dependence of microwave backscattering from the sea and the moon with those of light backscattered from fabricated rough surfaces. When the microwave backscattering was scaled down to optical backscattering dimensions, they obtained a good agreement. Jordan [31] carried out measurements of optical backscattering from fabricated two-dimensional (2D) rough surfaces (gold-coated dry-honing silicon wafers). He compared his results with radar sea scattering data as well as with the predictions of Rice's perturbation theory [12], although, as he pointed out, the surfaces used in his work were too rough to comply with the limitations of a perturbation approach.

The work reported in this article is an experimental investigation of the light backscattered from well-characterized double-scale surfaces, i.e., surfaces having a small-scale random component superimposed on a large-scale periodic grating, illuminated at small and large angles of incidence.

It shows some trends in the scattering behavior and provides physical insight on the scattering processes occurring for composite rough surfaces that provide ground for the testing of two-scale theoretical approaches.

Furthermore, the experimental work reported here can be related to a scaled-down sea scattering situation; that is, it is possible to undertake laboratory optical frequency experiments to investigate the in-plane angular scattering properties of fabricated oceanlike surfaces, with well controlled statistical parameters, that may aid in the understanding of the features of radar sea scattering.

2. MODELING THE DOUBLE-SCALE SURFACES

For our experimental study, we shall consider double-scale surfaces that can be modeled as a superposition of two independent components: a small-amplitude, high-frequency roughness and a low-frequency, large amplitude component. The latter may be a periodic surface. These kind of surfaces can be related, as we mentioned earlier, to oceanlike surfaces, where the wind-driven sea is best thought of as random ripples (capillary waves) on top of large gravity waves.

Therefore, in modeling our oceanlike surfaces, we shall consider the mathematical description employed for sea surface waves, with two cases being considered for the large amplitude component: a sine wave and a Stokes wave of the fourth order.

A simple theory that considers the sea surface as a single sinusoidal wave cannot completely describe real ocean waves, although this approach has had success in describing, with considerable accuracy, the basic dynamics of their propagation. The fact that for small-amplitude waves the linear theory is adequate has encouraged the adoption of the pragmatic approach of regarding the irregular sea surface as a composite of many ideal sinusoidal wave components [25].

Thus, the first model for the slow-varying, large amplitude component (gravity wave) is a large-scale surface with a sinusoidal profile. The gravity wave is thus given by [25,32,33]

$$\zeta(x) = A_p \sin(Kx), \tag{1}$$

where $K = 2\pi/\Lambda$ is the wavenumber, Λ is the period, and A_p is the amplitude of the wave. A condition for the validity of the linear wave solution considered above is that the wave slope be small ($A_p/\Lambda < 1/7$) [33].

Whilst the linear wave theory is adequate for many applications, it may be necessary to model the sea more closely with nonlinear solutions. This is because the basic dynamics are in fact nonlinear, and the linear solution represented by Eq. (1) is only an approximation. Therefore, as a second model for the large-scale surface, we shall consider a Stokes wave of the fourth order, which is a nonlinear solution to the wave theory [25,32,33]. A Stokes wave is a series solution expressed as an infinite power series in terms of a parameter related to the slope (A_p/Λ). For the fourth order solution, the sea wave profile is given by [25]

$$\zeta(x) = -A_p \cos(Kx) + \left(\frac{1}{2}KA_p^2 + \frac{17}{24}K^3A_p^4\right)\cos(2Kx) - \frac{3}{8}K^2A_p^3\cos(3Kx) + \frac{1}{3}K^3A_p^4\cos(4Kx). \tag{2}$$

As has been mentioned, the small-scale surface component can be related to random ripples (capillary waves), riding on top of the large gravity waves of the sea surface. If the ripples are formed from many contributions arising from relatively unrelated forces, it is then reasonable to assume these contributions to be statistically independent. The distribution of ripple heights, arising from the summation of all these independent contributions, is thus assumed to be Gaussian. A fully developed sea falls into this category. For most purposes, the Gaussian distribution is satisfactory, although in the context of radar imaging, the skewness of the height distribution may be important. From the experimental point of view, it is more convenient to consider a Gaussian distribution, since a technique for fabricating this kind of surface is readily available [34]. Therefore, we shall consider a Gaussian process for the random ripples (small-scale roughness) riding on top of gravity waves, with σ_ζ as the standard deviation of heights of the capillary waves. In our surface model, we also consider the autocorrelation function of ripple heights of two points at different positions at a fixed time to be a Gaussian function, whose exp −1 value a is the correlation length.

3. SURFACE FABRICATION

Several methods have been proposed for the manufacture of very well-characterized scattering surfaces [9,28,34,35] and some aspects of our fabrication techniques are similar to the ones employed in those works.

We have carried out experiments in the laboratory at optical frequencies, scaling down the problem of radar scattering from sea surfaces. For this, we make the following considerations.

We model the waves of the ocean surface as a composition of small-random waves on top of long-period waves (gravity waves), as mentioned in the last section. Since most of the probing of the ocean surface nowadays is made with radar, we choose to model radar experiments in the C band of the microwave spectrum (6.0 cm wavelength), scaling down the problem to the optical regions in which we use the 0.633 μm line of a He–Ne laser. We shall consider a fully developed sea with no borders (no coast lines) having, according to our sea surface model, a large (gravity) wave period of 100.0 m and a wave height (distance between the wave crest and the wave trough) of 5.0 m. We shall also consider small-random capillary waves with a standard deviation of the order of 10 cm and an correlation length of the order of 20.0 cm. As mentioned at the end of Section 2, for this small-scale roughness, we are considering a Gaussian distribution in heights and a Gaussian autocorrelation function of heights.

To perform the laboratory optical frequency experiments and investigate the in-plane angular scattering properties, four large-scale composite randomly rough surfaces were manufactured.

These are basically large-scale, slow-varying diamond-machined periodic surfaces made on 5.0 cm by 5.0 cm aluminum blanks. Two of the surfaces have a sinusoidal profile [Eq. (1)] with a period of $\Lambda = 1.0$ mm and a peak-to-valley height of $2A_p = 50.0$ μm. Those parameters are scaled down from our original sea surface. The other two long-period surfaces have a Stokes wave profile of the fourth order (described by Eq. (2)), where the period is $\Lambda = 1.0$ mm and the peak-to-valley height is 50.0 μm.

In order to include the small-scale, randomly rough surface on top of the large-scale periodic surface, we used the speckle technique for surface manufacturing described in Gray [34] and Ruiz-Cortés and Dainty [36]; first, a photoresist coating is applied by an immersion technique, and then the small-scale roughness with the desired properties is imposed by a photo-etching procedure. After the photo-fabrication procedure, the surfaces were coated with a thin layer of gold using the vacuum vapor deposition technique. Details of the fabrication technique can be found in [36]. The parameters for the small-scale random surface that correspond to those of the original sea surface are a standard deviation of around 1.0 μm and a correlation length of around 2.0 μm. Another important parameter to consider to compare our results with radar scattering is the dielectric constant. In the case of sea water at 20.0 °C with a salinity of 35% frequency of 5Ghz, the dielectric constant is $\epsilon = -65.09 + i33.61$ [37], and for gold at 0.633 μm it is $\epsilon = -62.79 + i4.95$ [38]. This parameter cannot be scaled.

The characterization of the surfaces was carried out using two profilometers. We first used a Rank Taylor–Hobson TalySurf model 112/0. This TalySurf has enough vertical and horizontal dynamic range to measure the main features of the large-scale component without having problems of nonlinearity. To measure the small-component roughness we used a Rank Taylor–Hobson TalyStep model 223-7. This TalyStep has a much higher resolution than the previous one. We took several scans along the grooves of the large-scale surface over three different regions, crest, trough ,and middle part (a region between the peak and the valley), and averaged the parameters so obtained.

Figure 1 shows the traces for the surfaces with a sinusoidal profile, while Fig. 2 shows the traces for the surfaces for the Stokes waves of the fourth order. It is worthwhile noting the difference between the two kinds of slow-varying periodic surfaces.

Table 1 shows the parameters for the large and small features of the two large-scale composite randomly rough surfaces. As we can see, the standard deviation of heights of the small-scale component is not the same in the three regions. The surfaces are rougher at the trough. Also, due to the thickness of the photoresist layer, the peak-to-valley heights are shorter than those of the uncoated aluminum substrates.

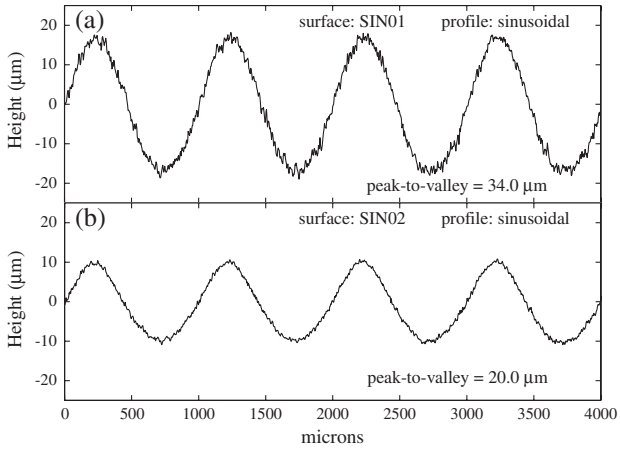

Fig. 1. TalyStep profile traces taken from double-scale surfaces with sinusoidal profile. Upper plot (a), surface SIN01 with a standard deviation of heights of $\sigma_\zeta = 1.0$ μm and a $1/e$ autocorrelation width of $a = 3.70$ μm for the small-scale component. Lower plot (b), surface SIN02 with a standard deviation of heights of $\sigma_\zeta = 0.56$ μm and a $1/e$ autocorrelation width of $a = 2.17$ μm for the small-scale component.

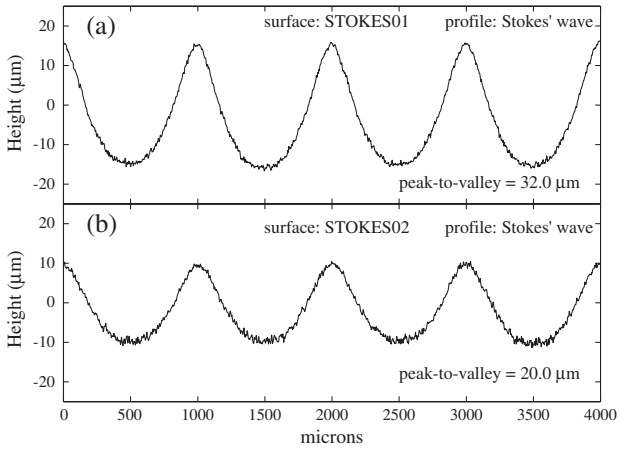

Fig. 2. TalyStep profile traces taken from double-scale surfaces with Stokes wave profile. Upper plot (a), surface STOKES01 with a standard deviation of heights of $\sigma_\zeta = 0.56$ μm and a $1/e$ autocorrelation width of $a = 2.49$ μm for the small-scale component. Lower plot (b), surface STOKES02 with a standard deviation of heights of $\sigma_\zeta = 0.73$ μm and a $1/e$ autocorrelation width of $a = 2.22$ μm for the small-scale component.

4. EXPERIMENTAL SETUP

The diagram of the experimental arrangement for the measurements of backscattering is presented in Fig. 3; the arrangement is similar to the setup reported in [31]. A polarized beam of wavelength $\lambda = 0.6328$ μm from a 5.0 mW helium-neon laser was used to illuminate the surfaces. In order to minimize the noise level, the beam was chopped at 800 Hz, and the signal of the chopper was fed, together with the detector signal, to a lock-in amplifier. The laser beam was passed through a half-wave plate, whose rotation allowed for the change of the incident field polarization. That is, the rough surface could be illuminated with an s or a p polarized beam. To avoid illuminating the edges of the surface at large angles of incidence, the width of the beam was of 3.0 mm at the center of the rotating stage. In order to measure the light scattered in the exact retro-reflection direction, a beam-splitter was used. The beam passed through the beam-splitter and illuminated the rough surface, the light coming back in the opposite direction (backscattered) being redirected by the beam-splitter towards a photo-multiplier detector. The beam-splitter was a nonpolarizing dielectric cube having a reflectivity for s and p polarized light of 50.0% matched to within 3.0% (manufacturer specifications). The rough surfaces were mounted on a computer-controlled rotating stage in order to change the angle of incidence. An integrating lens was placed in front of the detector for collecting and spatially averaging speckles over a fixed solid angle in order to reduce the random noise. An analyzer in front of the detector made it possible to measure to co- and cross-polarized components of the backscattered light. Care was taken to place the detector in the exact backscattering direction, and also to avoid illuminating the edges of the surface, especially at very large angles of incidence.

Because it is more convenient to study the angular dependence of backscattering data normalized to unity at normal incidence, we shall present our results as the normalized

Table 1. Surface Parameters for the Large and Small Component of the Double-Scale Randomly Rough Surfaces

	Large scale		Small scale	
Surface	Period (mm)	Peak-to-valley (μm)	Average standard deviation σ (μm)	Average correlation length a (μm)
SIN01	1.0	34.0 ± 0.02	1.0 ± 0.03	3.70 ± 0.12
SIN02	1.0	20.0 ± 0.01	0.56 ± 0.02	2.17 ± 0.07
STOKES01	1.0	32.0 ± 0.01	0.56 ± 0.02	2.49 ± 0.08
STOKES02	1.0	20.0 ± 0.02	0.73 ± 0.02	2.22 ± 0.07

backscattered intensity (I_{nbs}) as a function of the angle of incidence; that is (after Renau and Collinson [29]),

$$I_{\mathrm{nbs}} = \frac{I_{\mathrm{bs}}(\theta_{\mathrm{inc}})}{I_{\mathrm{bs}}(0)}, \tag{3}$$

where $I_{\mathrm{bs}}(\theta_{\mathrm{inc}})$ is the scattered intensity in the backscattering direction.

Repeated measurements of the scattered light from the same rough surface were extremely reproducible. To further reduce the speckle noise in this case, many measurements were made with the sample translated by a distance, along the grooves, sufficiently large to cause partial decorrelation between successive regions of the surface exposed to the illuminating narrow beam, and the results were averaged.

5. RESULTS

In this section, we shall examine the behavior of the measurements of the backscattered light and relate them to the statistical characteristics of the scattering surfaces.

We shall present the experimental results of the normalized backscattered intensity, as a function of the angle of incidence [Eq. (3)], for the four large-scale composite random rough surfaces that were manufactured. In what follows, the circles (○) are for the copolarized component and the diamonds (◇) are for the cross-polarized component of the scattered light when the surface was illuminated with an *s* polarized incident field, that is, the *ss* and *sp* components, respectively. Triangles (Δ) are for the copolarized component (*pp*), and the asterisks (∗) are for the cross-polarized component (*ps*) when the surface was illuminated with a *p* polarized incident field.

The surfaces were oriented so that the plane of incidence was perpendicular to the grooves of the large-scale periodic surface.

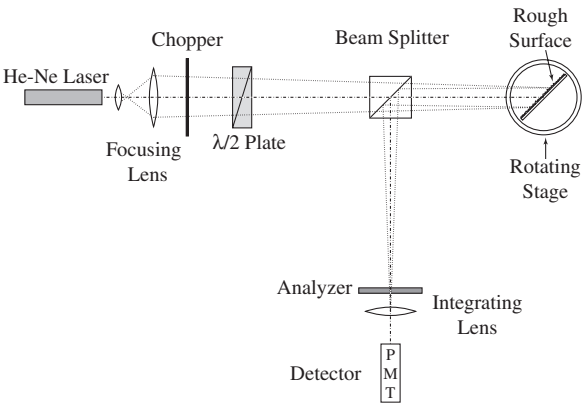

Fig. 3. Schematic representation of the apparatus used for experimental backscattering measurements.

Figure 4 shows the normalized backscattered intensity from surface SIN01. The cross-polarized components (*sp* and *ps*) follow an almost identical behavior for all angles of incidence. However, the copolarized components (*ss* and *pp*) show similar behaviors up to 20° of incidence; after that, the *pp* component falls slower than the *ss* component as the angle of incidence increases. Starting at 20° and up to approximately 70°, the difference between the two copolarized components is more evident. The normalized backscattered intensity decreases with a negative curvature (up to 20.0°) with angle. From $\theta_{\mathrm{inc}} = 20.0°$ and up to around $\theta_{\mathrm{inc}} = 40.0°$, the rate decreases. From around 40.0° of incidence, the fall is faster, and then it changes curvature at around 60.0° of incidence and continues decreasing slowly.

In Fig. 5, we present the experimental measurements of the normalized backscattered intensity from surface SIN02. As for the previous surface, the cross-polarized components show an almost identical scattering pattern of behavior. However, when we compare the copolarized components, it can be seen that, again, the *pp* component decreases at a slower rate than the *ss* component. This difference is noticeable from around 5.0° of incidence. The falling rate remains more or less constant up to an angle of incidence of 40.0°, after which the normalized backscattered intensity falls off rapidly. Then, it changes curvature at around 60.0° of incidence and keeps decreasing slowly.

The normalized backscattered intensity for surface STOKES01 is shown in Fig. 6. Again, a tendency for the *pp* component to exhibit a slower fall with angle of incidence is present. The strength of the backscattered intensity from normal incidence up to 15.0° of incidence has a falling rate that slows down from 15.0° up to approximately 40.0°, where

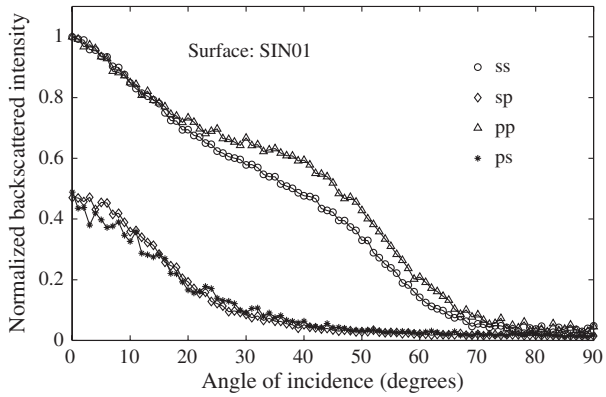

Fig. 4. Experimental measurements of the angular distribution of the normalized backscattered intensity from surface SIN01. In circles (○) the *ss* component, diamonds (◇) the *sp* component, triangles (Δ) the *pp* component, and asterisks (∗) the *ps* component.

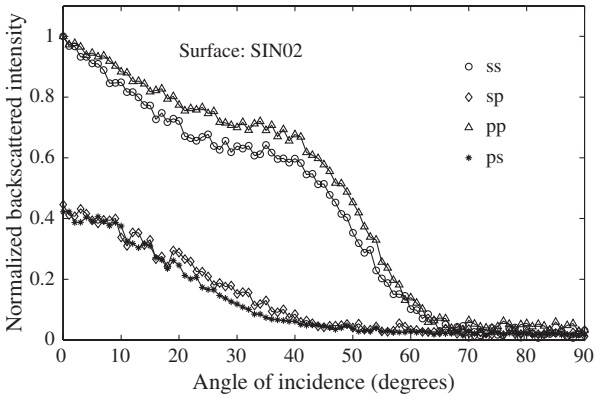

Fig. 5. Experimental measurements of the angular distribution of the normalized backscattered intensity from surface SIN02. In circles (○) the *ss* component, diamonds (◇) the *sp* component, triangles (Δ) the *pp* component, and asterisks (∗) the *ps* component.

there seems to be a plateau region; then if falls rapidly from 40.0° to 60.0°, and then keeps decreasing slowly.

The behavior of the cross-polarized components seems to be nearly identical to that of the previous surfaces, and the degree of depolarization reaches about 50.0% of the copolarized component strength at normal incidence.

Figure 7 shows the experimental measurements of the normalized backscattered intensity for surface STOKES02. As before, the *pp* component presents a slower rate of fall up to approximately 55.0°; both copolarized components follow a similar behavior.

The copolarized backscattering components have a broader envelope and also seem to show a plateau region in the interval of angle of incidence $15.0° < \theta_{\text{inc}} < 60.0°$. The falling rate increases rapidly starting from 60.0° and up to 80.0° and then decreases at a slower rate. A very small difference in the normalized backscattered intensity behavior near normal incidence for the cross-polarized components is also present. For angles of incidence larger than 10° the behavior is similar.

In order to investigate with more detail the nature of the backscattered intensity, we shall study the polarization structure of the backscattered light.

For linearly polarized incident light, it was found that the backscattered radiation consisted of a linearly polarized

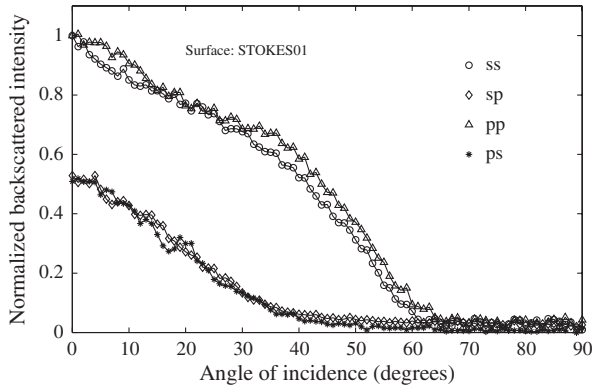

Fig. 6. Experimental measurements of the angular distribution of the normalized backscattered intensity from surface STOKES01. In circles (○) the *ss* component, diamonds (◇) the *sp* component, triangles (Δ) the *pp* component, and asterisks (∗) the *ps* component.

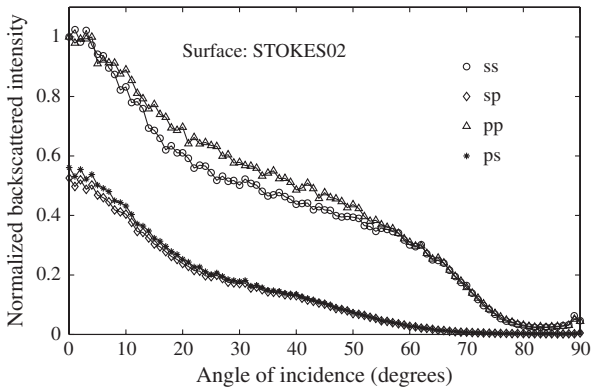

Fig. 7. Experimental measurements of the angular distribution of the normalized backscattered intensity from surface STOKES02. In circles (○) the *ss* component, diamonds (◇) the *sp* component, triangles (Δ) the *pp* component, and asterisks (∗) the *ps* component.

and a depolarized component [30]. The linearly polarized backscatter component has the same polarization as the incident field. The depolarized component did not show a preferred polarized direction.

Following Dainty *et al.* [39], Kim *et al.* [15], and Renau *et al.* [30], we shall describe the backscattered light in terms of polarized ($I_{\text{bs-pol}}$) and depolarized polarized $I_{\text{bs-dpol}}$ components, and not just in terms of co- and cross-polarised components. Assuming an *s* polarized incident beam, it can be shown ([39], [15], and [30]) that the polarized and depolarized normalized backscattered intensities are given by

$$I_{\text{nbs-pol}} = \frac{I_{\text{bs-}ss}(\theta_{\text{inc}}) - I_{\text{bs-}sp}(\theta_{\text{inc}})}{I_{\text{bs-}ss}(0)}, \tag{4}$$

and

$$I_{\text{nbs-dpol}} = \frac{2I_{\text{bs-}sp}(\theta_{\text{inc}})}{I_{\text{bs-}ss}(0)}, \tag{5}$$

where $I_{\text{bs-}ss}(\theta_{\text{inc}})$ and $I_{\text{bs-}sp}(\theta_{\text{inc}})$ are the backscattered intensities for the copolarized (*ss*) and cross-polarized (*sp*) components, respectively.

As an outcome of the previous result, we present in Figs. 8 and 9 the normalized backscattered intensity of the polarized component (dotted line), the depolarized component (dashed line), and the copolarized (*ss*) component (circles) for the surfaces with sinusoidal and Stokes wave profile, respectively.

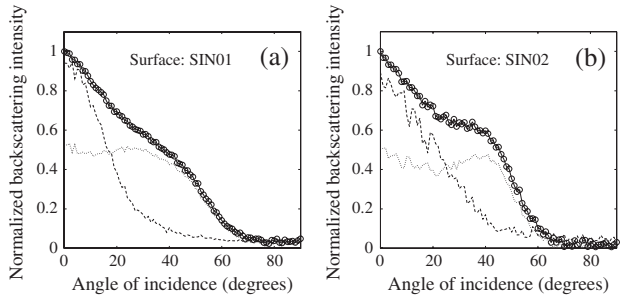

Fig. 8. Normalized backscattered intensity of the polarized and depolarized components. Dotted line: the polarized component. Dashed line: the depolarized component. Circles: the copolarized (*ss*) component.

According to the model presented by O'Donnell and Méndez [9], light singly scattered has a preferred polarization, and multiple scattering is the reason of depolarization. Kim *et al.* [15] and Dainty *et al.* [39] found that, to a first approximation, the polarized component is the result of single scattering and the depolarized component is the result of multiple scattering. Therefore, according to the multiple scattering model [9], the enhanced backscattered contribution to the scattering of light is the depolarized component.

Keeping the previous statement in mind, it can be seen that in Fig. 8, the depolarized component (enhanced backscattering contribution) is prominent from 0° of incidence up to around 25° of incidence for surface SIN01 [Fig. 8(a)] and from 0° of incidence up to around 35° of incidence for surface SIN02 [Fig 8(b)]. For the polarized component, significant scattering is observed from normal incidence up to 40° for surface SIN01 and 45° for surface SIN02 and then falls off rapidly for both surfaces. Towards grazing incidence ($\theta_{inc} > 65°$), the backscattered intensity is very small for both surfaces.

For the surfaces with a Stokes wave profile, Fig. 9, the depolarized component (enhanced backscattering contribution) is prominent from 0° of incidence up to around 35° of incidence for surface STOKES01 [Fig. 8(a)], and from 0° of incidence up to around 45° of incidence for surface SIN02 [Fig. 9(b)]. For the polarized component, significant scattering is observed from normal incidence up to 40° for surface STOKES01 and 60° for surface STOKES02 and then falls off rapidly for both surfaces. Towards large angles of incidence, 60° for surface STOKES01 and 80° for surface STOKES02, the backscattered intensity is very small.

Therefore, we can identify, empirically, three regions in which different mechanisms seem to contribute to the backscattered intensity. First, a region near normal incidence, where multiple scattering processes (depolarized component) seem to produce the largest contribution to the backscattered intensity. Then, a region away from normal incidence (starting from about 20° of incidence), where the polarized component seems to be the main contributor to the backscattered intensity and we associate this region with single scattering; therefore, we shall identify this as a diffuse region. Finally, at large angles of incidence, we identify a region where the backscattering intensity falls off rapidly and where shadowing effects become significant.

The above criteria are in agreement with the published literature [3,26,40,41] in the conjectures that describe the three scattering regions that predominate in radar backscattering from the ocean at various angles of incidence. Also, comparison with theoretical studies such as the two-scale model [19] and the small-slope approximation [27] shows that our experimental data are consistent with numerical results obtained on the basis of these two methods.

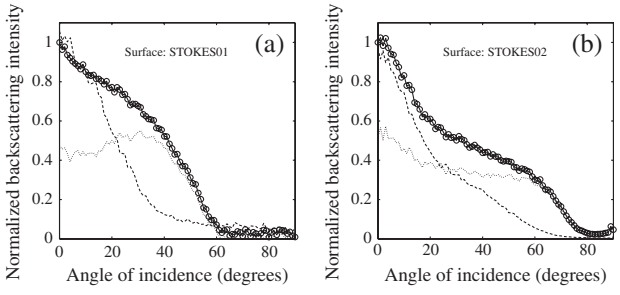

Fig. 9. Normalized backscattered intensity of the polarized and random polarized components. Dotted line: the polarized component. Dashed line: the depolarized component. Circles: the copolarized (*ss*) component.

6. CONCLUSIONS

Experimental measurements of backscattered light from large-scale composite random rough surfaces (oceanlike surfaces) were presented. These surfaces are a composition of a small-random component riding on top of a large-scale surface component.

The backscattered light was also decomposed into contributions from their polarized and depolarized components. We identified three regions in which different mechanisms seem to contribute to the backscattered intensity. Firstly, a region near normal incidence, where multiple scattering processes (unpolarized component) seem to produce the largest contribution to the backscattered intensity. Then, a region away from normal incidence, where the polarized component seems to be the main contributor to the backscattered intensity; we, therefore, associate this region with single scattering. Finally, at large angles of incidence, we identified a region where the backscattering power falls off rapidly, and where shadowing effects become significant.

ACKNOWLEDGMENTS

VRC would like to thank the Consejo Nacional de Ciencia y Tecnología (CONACyT) and the Centro de Investigación Científica y Educación Superior de Ensenada (CICESE), both in Mexico, for their financial support. JCD acknowledges the support of the Science Foundation of Ireland under grant 07/IN.1/I906

REFERENCES

1. D. A. Zimnyakov and V. V. Tuchin, "Optical tomography of tissues," Quantum Electron. **32**, 849–867 (2002).
2. J. B. Campbell, *Introduction to Remote Sensing* (Guilford Press, 2006).
3. G. R. Valenzuela, "Theories for the interaction of electromagnetic and oceanic waves—a review," Boundary-Layer Meteorol. **13**, 61–85 (1978).
4. Y. Inouye and S. Kawata, "Near-field scanning optical microscope with a metallic probe tip," Opt. Lett. **19**, 159–161 (1994).
5. J. F. Aguilar and E. R. Méndez, "Imaging optically thick objects in scanning microscopy: perfectly conducting surfaces," J. Opt. Soc. Am. A **11**, 155–167 (1994).
6. J. M. Bennett and L. Mattsson, *Introduction to Surface Roughness and Scattering* (Optical Society of America, 1999).
7. N. J. Elton, "A two-scale roughness model for the gloss of coated paper," J. Opt. A **10**, 085002 (2008).
8. E. R. Méndez and K. A. O'Donnell, "Observation of depolarization and backscattering enhancement in light scattering from Gaussian random surfaces," Opt. Commun. **61**, 91–95 (1987).
9. K. A. O'Donnell and E. R. Méndez, "Experimental study of scattering from characterized random surfaces," J. Opt. Soc. Am. A **4**, 1194–1205 (1987).
10. P. Beckmann and A. Spizzichino, *The Scattering of Electromagnetic Waves from Rough Surfaces* (Pergamon, 1963).
11. J. A. Ogilvy, *Theory of Wave Scattering from Random Rough Surfaces* (Hilger, 1991).
12. S. O. Rice, "Reflection of electromagnetic waves from slightly rough surfaces," Commun. Pure Appl. Math. **4**, 351–378 (1951).
13. A. A. Maradudin, T. Michel, A. R. McGurn, and E. R. Méndez, "Enhanced backscattering of light from a random grating," Ann. Phys. **203**, 255–307 (1990).

14. A. Mendoza and E. Méndez, "Light scattering by a reentrant fractal surface," Appl. Opt. **36**, 3521–3531 (1997).
15. M. J. Kim, J. C. Dainty, A. T. Friberg, and A. J. Sant, "Experimental study of enhanced backscattering from one and two dimensional random rough surfaces," J. Opt. Soc. Am. A **7**, 569–577 (1990).
16. M. E. Knotts, "Experimental studies of multiple scattering by rough surfaces," Ph.D. thesis (Georgia Institute of Technology, 1994).
17. A. J. Sant, "Enhanced backscattering of light from randomly rough diffusers," Ph.D. thesis (Imperial College, University of London, 1990).
18. J. A. DeSanto, "Theoretical methods in ocean acoustics," in *Ocean Acoustics*, J. A. DeSanto, ed. (Springer-Verlag, 1979).
19. M. Y. Ayari, A. Khenchaf, and A. Coatanhay, "Simulations of the bistatic scattering using two-scale model and the unified sea spectrum," J. Appl. Remote Sens. **1**, 013532 (2007).
20. J. T. Johnson, R. T. Shin, J. A. Kong, L. Tsang, and K. Pak, "A numerical study of the composite surface model for ocean backscattering," IEEE Trans. Geosci. Remote Sens. **36**, 72–83 (1998).
21. H. D. Mouche and V. Kudryavtsev, "Radar scattering of the ocean surface and sea-roughness properties: a combined analysis from dual-polarizations airborne radar observations and models in C band," J. Geophys. Res. Oceans **111**, C09004 (2006).
22. W. J. Plant, "A stochastic, multiscale model of microwave backscatter from the ocean," J. Geophys. Res. **107**, 3120 (2002).
23. G. Soriano and C.-A. Guérin, "A cutoff invariant two-scale model in electromagnetic scattering from sea surfaces," IEEE Geosci. Remote Sens. Lett. **5**, 199–203 (2008).
24. M. Zhang, D. Nie, and H.-C. Yin, "A versatile composite surface model for electromagnetic backscattering from seas," Waves Random Complex Media **21**, 348–361 (2011).
25. B. Kinsman, *Wind Waves: Their Generation and Propagation on the Ocean Surface* (Prentice-Hall, 1965).
26. A. Fung and H. L. Chan, "Backscattering of waves by composite rough surfaces," IEEE Trans. Antennas Propag. **AP-17**, 590–597 (1976).
27. A. Voronovich and V. U. Zavorotny, "Theoretical model for scattering of radar signals in K_u—and C-bands from a rough sea surface with breaking waves," Waves Random Media **11**, 247–269 (2001).
28. M. J. Kim, "Light scattering from characterised random rough surfaces," Ph.D. thesis (Imperial College, University of London, 1989).
29. J. Renau and J. A. Collinson, "Measurements of electromagnetic backscattering from known rough surfaces," Bell Syst. Tech. J. **44**, 2203–2226 (1965).
30. J. Renau, P. K. Cheo, and H. G. Cooper, "Depolarisation of linearly polarised electromagnetic waves backscattered from rough metals and inhomogeneous dielectrics," J. Opt. Soc. Am. **57**, 459–467 (1967).
31. D. L. Jordan, "Experimental measurements of optical backscattering from surfaces of roughness comparable to the wavelength and their application to radar sea scattering," Waves Random Media **5**, 41–54 (1995).
32. P. A. Le Blond and L. A. Mysak, *Waves in the Ocean* (Elsevier, 1978).
33. I. S. Robinson, J. O. Thomas, K. Ouchi, and Y. C. Robertson, *Study of the Sea Surface, Ocean Waves and Dynamics with Special Reference to Synthetic Aperture Radar (SAR) Imagery* (Oxford Computer Services, 1981).
34. P. F. Gray, "A method of forming optical diffusers of simple known statistical properties," Opt. Acta **25**, 765–775 (1978).
35. K. A. O'Donnell and M. E. Knotss, "Polarization-dependence of scattering from one-dimensional rough surfaces," J. Opt. Soc. Am. A **8**, 1126–1131 (1991).
36. V. A. Ruiz-Cortés and J. C. Dainty, "Experimental light-scattering measurements from large-scale composite randomly rough surfaces," J. Opt. Soc. Am. A **19**, 2043–2052 (2002).
37. A. Stogryn, "Equations for calculating the dielectric constant of saline water," IEEE Trans. Microwave Theory Tech. **19**, 733–736 (1971).
38. P. B. Johnson and R. W. Christy, "Optical constants of the noble metals," Phys. Rev. B **6**, 4370–4379 (1972).
39. J. C. Dainty, M. J. Kim, and A. J. Sant, "Measurements of angular scattering by randomly rough metal and dielectric surfaces," in *Scattering in Volumes and Surfaces*, M. Nieto-Vesperinas and J. C. Dainty, eds. (Elsevier Science, 1990).
40. D. E. Barrick and W. H. Peake, "A review of scattering from surfaces with different roughness scales," Radio Sci. **3**, 865–868 (1968).
41. A. K. Fung, "Surface scattering effects at different spectral regions," in *Spectral Signatures of Objects in Remote Sensing*, G. Guyot and M. Verbrugghe, eds. (INRA, 1984) pp. 693–707.